On single-crystal neutron-diffraction in DACs: quantitative structure refinement of light elements on SNAP and TOPAZ

ARTICLE TEMPLATE

On Single-Crystal Neutron-Diffraction in DACs: Quantitative Structure Refinement of Light Elements on SNAP and TOPAZ

B. Massani[a], J. S. Loveday[a], J. J. Molaison[b], A. M. dos Santos[b], X. P. Wang[b], L. L. Daemen[b], B. Haberl[b], R. Boehler[b], and M. Guthrie[a,c]

[a]SUPA, School of Physics and Astronomy, and Centre for Science at Extreme Conditions, The University of Edinburgh, Edinburgh EH9 3FD, United Kingdom;
[b]Neutron Scattering Division, Neutron Sciences Directorate, Oak Ridge National Laboratory, Oak Ridge, TN 37830, USA;
[c]European Spallation Source, ERIC, Lund, Sweden

ARTICLE HISTORY
Compiled June 26, 2020

ABSTRACT
Quantitative single crystal neutron-diffraction in diamond anvil cells has so far been to limited by the neutron flux available at the various neutron sources. As a result, highly precise measurements of the exact position of light elements have not been possible preventing, for example, structural studies of hydrogen and hydrogen bonds under pressure. Here we report experiments carried out on SNAP at the Spallation Neutron Source (ORNL, TN, USA) to explore the possibility and current limits of such studies. Furthermore, we benchmarked the obtained data quality with reference experiments carried out on TOPAZ, a dedicated single-crystal instrument.
We show that measuring single-crystal diffraction intensities on SNAP is possible to such a precision that we are able to resolve the hydrogen bonds in potassium dideuterium phosphate (DKDP) as well as in ice VI.

KEYWORDS
Single-Crystal; Neutron-Diffraction; H-bonds; DAC; SNAP; TOPAZ

1. Introduction

The crystal structures of many important simple-molecular systems - such as hydrogen/deuterium, ammonia, methane, ice - are surprisingly poorly understood under high pressure. For example, solid, compressed hydrogen is the most abundant substance in our solar system, yet not even the H-H bondlength was directly measured at any elevated pressure and the space group of the high-pressure phases remain unknown (Goncharenko & Loubeyre, 2005). Similarly, ice, ammonia, methane, and their binary and ternary mixtures exhibit a wealth of phases and phenomena such as H-bond centring and superionicity (Cavazzoni et al., 1999; Millot et al., 2018), all materials which are poorly characterised from a structural point of view.

Accurate structural information on these systems is vital to solve a wide range of scientific problems. The outer solar system is dominated by hydrogen and hydrogen-rich materials and knowledge of their high-pressure structures is vital to develop models of phenomena such as the existence and strength of magnetic dynamos, the internal structure of gas-giants & moons, and even to the evolution and composition

of atmospheres (Bezacier et al., 2013; Guillot, 2005; Helled, Anderson, Podolak, & Schubert, 2011; Hubbard, 1997; Loveday & Nelmes, 2003; Shin, Kumar, Udachin, Alavi, & Ripmeester, 2012; Tobie, Grasset, Lunine, Mocquet, & Sotin, 2005). The long-standing problem of the formation of metallic hydrogen is an important model for the behaviour of solids when quantum effects become significant (Cui, Chen, & Silvera, 1995; Geneste, Torrent, & Loubeyre, 2012; Mao & Hemley, 2001; Silvera, 1980). The behaviour of protons in H-bonded systems like ice are proxys for more complex biological systems (see for example (*et al.*, 2002)). Finally, the recent discovery of high temperature superconductivity in hydrogen-rich systems like hydrogen sulphide and lanthanum super-hydride provides further need for accurate structural information at high pressure. The superconductivity is believed to be driven by the high polarisability of the hydrogen atoms, which leads to strong electron-phonon coupling with high coupling frequencies (Chen et al., 2010; Drozdov, Eremets, Troyan, Ksenofontov, & Shylin, 2015; Duang et al., 2014; Gao et al., 1994). However, to date, no full structure (including hydrogen positions) of a hydrogen-rich high-temperature superconductor has been determined.

The small scattering cross-section of hydrogen for X-rays makes neutron diffraction the only reliable method to exactly measure the proton (or deuteron) positions in a crystal structure. Such measurements were the first to verify the model of hydrogen bonds proposed by Pauling (1935) and by Wollan, Davidson, and Shull (1949) and revealed the familiar bent shape of the water molecule in ice I_h (Wollan et al., 1949). However, until the advent of bright spallation sources, the measurement of neutron powder patterns of sufficient quality for structural refinement has been limited in pressure to 25 GPa due to the large sample volumes required. Some classic examples of large volume devices used at neutron facilities around the world include gas pressure cells ($P_{max} \sim 0.7$ GPa), clamp cells ($P_{max} \sim 2$ GPa), and the Paris-Edinburgh presses ($P_{max} \sim 30$ GPa) (cf. Besson et al. (1992); Klotz (2013)).

Recent developments in diamond synthesis have paved the way for larger diamonds and with this large-volume diamond anvil cells (DAC) (Boehler et al., 2013; Haberl et al., 2018; R. Boehler *et al.*, 2017). Combined with extremely bright neutron sources, available at the Spallation Neutron Source (SNS) a facility located in the Oak Ridge National Laboratory, neutron diffraction at a pressure up to 90 GPa has been demonstrated (Boehler et al., 2013; Guthrie et al., 2019). These DACs so far, have mainly been used for powder diffraction and, as such, information obtained from data has its limits. For many crystallographic studies, information from single-crystal techniques are vital in that they provide a much higher (real-space) resolution by enabling access to short d-spacing Bragg reflections that would heavily overlap in a powder study. At pressures >50 GPa powder methods, for example, give the same agreement indices for a 1-site and 2-site model of a hydrogen bond in high-pressure ice (cf. (Guthrie et al., 2019)) making it impossible to identify the better model. Of equal importance, single-crystal methods avoid the need to deuterate samples. The concentrated signal from sharp single-crystal Bragg spots remains visible on top of the incoherent scattering originating from protium ^{1}H that would overwhelm distributed powder intensities.

Use of DACs for high-pressure single-crystal neutron diffraction (HP-SCND) therefore paves the way for studies of hydrogen-rich systems to pressures currently inaccessible and with unprecedented structural detail.However, quantitative

single-crystal neutron diffraction (SCND) studies under high pressure in DACs remain challenging, albeit sucessful attempts that have been made. Binns, Kamenev, McIntyre, Moggach, and Parsons (2016) published a set of experiments at ANSTO's KOALA, a neutron Laue diffractometer, using a Merrill-Basset-type diamond cell with conical Boehler anvils ($\varnothing_{culet}$=1 mm). It demonstrated sufficient data quality for refinement on crystals of typical sizes for X-ray diffraction in a DAC. Furthermore, at Heinz Maier-Leibnitz Zentrum (MLZ)'s four- circle diffractometer HEiDi, monochromatic neutron diffraction was performed in a panoramic DAC with conical Boehler anvils and achieved high-quality data under compression to 1 GPa. Another successful test of the cell/anvil setup with 1.5 mm culets reached 7 GPa (Grzechnik, Meven, & Friese, 2018). These studies are mainly aiming for magnetic materials and large unit cells, but do not report a high enough diffraction resolution in the high-Q range to investigate H-bonds.
The goal of this study is to benchmark SNAP, a high-pressure time-of-flight diffractometer at the SNS for the quantitative structure analysis of single crystals containing hydrogen or other light elements in a DAC. As a reference, a similar set of experiment were carried out on TOPAZ, a dedicated single-crystal instrument also at the SNS. We will present a set of trial experiments to investigate the relationship between sample volume and data quality. These properties are inversely related to one another yet, unavoidably, the former is strictly limited in high-pressure studies. The systematic study of the crystallographic limitations of progressively smaller sample volumes is a critical first step in deployment routine quantitative single crystal structure refinement in a DAC.

Furthermore, we will show the influence of the complex sample environment consisting of diamonds and gasket on the data quality. To that end, we examined structural refinements of the deuterated ferroelectric potassium di-hydrogen phosphate (KD_2PO_4, DKDP), as a test case. DKDP is a classic example of a short hydrogen-bonded system, which has already been heavily studied with neutron diffraction – its structural properties are therefore well known up to modest pressures of about 2 GPa (Tibballs & Nelmes, 1982). Finally, we will test our data reduction procedure and all necessary corrections against a ice VI single-crystal grown *in-situ* under pressure in a diamond anvil cell.

2. Material and Methods

DKDP (KD_2PO_4), is a tetragonal body-centred crystal (space group $I\bar{4}2d$; N^o 122), with lattice parameters at ambient pressure and temperature of a=7.469(1) Å and b=6.976(1) Å (unit-cell volume 387.29 Å^3). A unit-cell contains four hydrogen-bonded formula units of KD_2PO_4, with all the hydrogen bonds lying in the ab-plane (Tibballs & Nelmes, 1982). The sample was synthesised at SNS by dissolving KDP (potassium dihydrogen-phasphate, KH_2PO_4) in D_2O and recrystallising out of solution. This procedure was repeated three times and two sample crystals were cut from the deuterated crystal. The larger of the two had a volume of 1.028 mm^3, and the small one had a volume of 0.028 mm^3 (disc-shaped; $\varnothing$=0.6 mm, h=0.1 mm). The latter volume was chosen because it matches the typical size and geometry of a sample chamber in diamond anvil cells for neutron diffraction (R. Boehler *et al.*, 2017).

Experiments were carried out at two SNS instruments: TOPAZ, the dedicated

single-crystal instrument and SNAP, the high-pressure beam line. TOPAZ is a high-resolution single-crystal diffractometer using the time-of-flight Laue technique with an array of neutron area detectors distributed spherically about the sample. The resulting angular coverage combined with a wide neutron wavelength band of 3.1 Å is well suited for efficient 3D-mapping of Bragg scattering in reciprocal space in the Q-range 0.45-25.00 Å^{-1}. As such, TOPAZ is well suited to determine atomic positions and displacement parameters of light elements, such as hydrogen. The high real-space resolution down to 0.25 Å, allows for precise measurements of atom-distances in H-bonds. Due to disorder both the paraelectric phase of DKDP and ice VI have average structures where the equivalent O-H$\cdots$O and the O$\cdots$H-O positions are occupied equally, resulting in a 50% occupancy on both sites, separated by a distance of less than 0.5 Å (Kuhs, Finney, Vettier, & Bliss, 1984; Wollan et al., 1949). A high real-space resolution is critical to resolve such a small displacement. Currently, TOPAZ has 24 of 48 detector ports populated with Anger camera modules covering about 3.0 sr in solid angle. TOPAZ uses a 18 m long bent focussing guide which focusses the beam to 2.0-4.0 mm. The high-precision goniometer is fixed to $X = 135^o$ and samples can be freely rotated about two axis, Φ and Ω (see figure 1)(Wang, Hoffmann, & dos Santos, 2018).

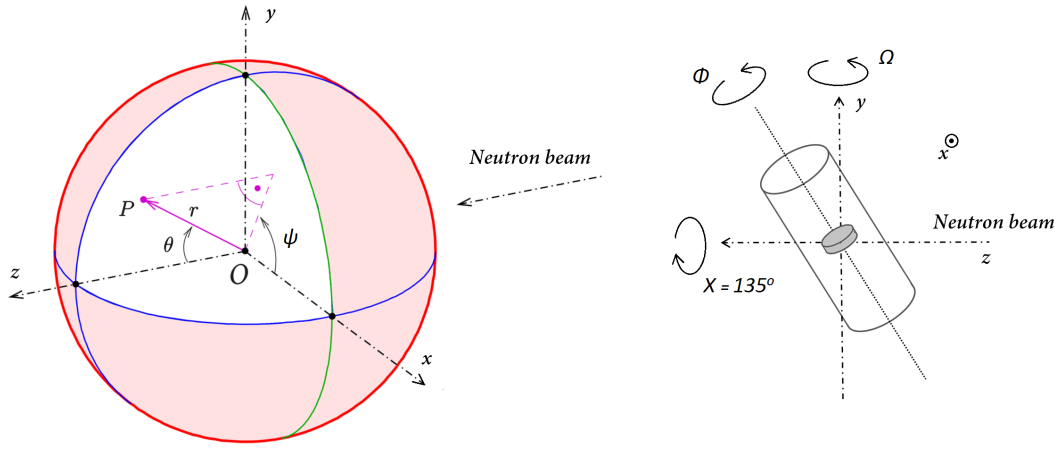

Figure 1. Left: Coordinate system on TOPAZ and SNAP. The beam direction is along the z-axis. The angle θ shown on between z and r is the scattering angle (twice the Bragg angle). The angles θ and Ψ give the direction of the diffracted beam. Right: The goniometer angles X, Φ, and Ω. On TOPAZ X is fixed to 135^o; on SNAP X and Φ are fixed to 0^o.

The Spallation Neutrons and Pressure (SNAP) instrument is a high-flux diffractometer primarily used for powder diffraction (Calder et al., 2018). SNAP uses area detectors of the same type as TOPAZ arranged in two 3x3 detector banks which allow for a Q-coverage of Q = 0.7-24.0 Å in the equatorial plane, depending on the detector positions (horizontal and vertical coverage: $\pm 22.5^o$). Compared to the neutron optics used on TOPAZ, the beam-focusing optics on SNAP are significantly shorter (guide length: 2.4 m; source-to-sample distance: 15 m), allowing for a high neutron flux at the expense of a higher divergence and complex beam profile. The instrument is hence well suited to deal with various complex sample environments for high-pressure studies. SNAP's capabilities for a full structural refinement of SCND data have so far not been tested.

SNS is operating at about 1.33 MW. The accumulated proton charge for the conducted experiments lay between $8.9 \cdot 10^{12}$ and $1.4 \cdot 10^{13}$. All data were normalised to the monitored proton current during the respective experiment.

Patterns of the bare crystals mounted on a Kapton-pin were collected for about 3 h per orientation both on SNAP and on TOPAZ. From this initial measurement on TOPAZ we were able to refine the deuteration ratio of the DKDP to be $> 94\%$. This compares well with that determined from the c/a ratio which is strongly dependent on the deuteration ratio Kuhs et al. (1984); Tibballs and Nelmes (1982).

Subsequently, the small crystal was placed in a DAC (SNAP) and a mock-DAC (TOPAZ). The mock-DAC was used because the sample stage on TOPAZ cannot support the weight of a real DAC. The DAC comprises a cell body made from hardened steel or beryllium-copper that drives two opposing diamonds together against the sample, which is contained by a metal gasket (for the detailed design see Haberl et al. (2018, 2017); R. Boehler *et al.* (2017).) The mock-DAC had the same basic parts but held together by a much lighter aluminium scaffolding instead of the heavy cell body. In both cases a circular, incident-beam collimator of 3 mm in diameter was chosen. The same collimator size was used to collect a Vanadium spectrum, a standard sample for the beam-profile calibration (see for example (Calder et al., 2018)). We then collected patterns of the crystal in the mock-DAC on TOPAZ for ten orientations (3x10h and 7x6h). Similarly, six orientations on SNAP were recorded (the sample rotation on SNAP is limited to a single vertical axis whereas TOPAZ has a two-axis orienter). The primary beam entered the cell through the gasket (see schematic sketch in figure 4). On SNAP data collection was limited to only 3 h collections per orientation.

In order to asses the methods developed here for SCND in a real DAC, a single-crystal of ice VI of a similar size as the small DKDP crystal was grown in a diamond anvil cell by repeatedly melting and re-crystalising a powder of ice VI in an ammonia-water pressure medium (Sigma-Aldrich, ND_4OD-D_2O, 25% , >99.99% deut.).

The data reduction was carried out using the Mantid data analysis and visualization package (Arnold et al., 2014). All crystallographic refinements were carried out using ExpGui(Toby, 2001), the graphical user interface for the Gsas-I software suite(Larson & Dreele, 2000).

3. Results and Discussion

3.1. Crystal Size: Effects on Data Quality

As a first step, we investigated the volume restrictions and the influence of the sample environment on the data quality using an instrument fully bench-marked for quantitative single crystal diffraction. To that end we measured the small, DAC-sized crystal on TOPAZ, the dedicated single crystal instrument at SNS. This marks the smallest crystal measured on this instrument to date. As mentioned above, ten orientations of the crystal were measured for 3 h each; each orientation contributed

about 100 reflections to the overall data set of 1044 reflections, after outliers had been removed as per standard procedure.

The structural refinement of the data set obtained from this experiment yielded values consistent with those reported in the literature, as obtained by Tibballs et al.(Tibballs & Nelmes, 1982). The respective structural information is given in table 4 (cf. appendix). This data set was used as a baseline for all subsequent measurements. In general, the deviation of the structural parameters from the literature values is very small and might be a feature introduced by a slightly different deuteration ratio of our sample compared to that of Tibballs *et al.* As mentioned above, the ratio of KDP ($a = 7.4521(4)$, $c = 6.974(2)$, $a/c = 0.936$) to DKDP ($a = 7.469(1)$, $c = 6.976(1)$, $a/c = 0.934$) has a large influence on the lattice parameter $a = b$; KDP expands more in the ab-plane than along the c-axis when deuterated. This behaviour is due to all the H-bonds being arranged in this plane. However, the obtained structural parameters are afflicted with larger errors of about one order of magnitude higher compared to the results published by Tibballs *et al.* Note that this is a direct result of the small sample volume, with the low intensites (high-Q) having a greater statistical uncertainty.
In general, our measurements are accurate but not as precise as the literature values. Still, these results show that even in a DAC-sized crystal it is possible to resolve the exact hydrogen/deuteron positions accurately on a well-calibrated neutron diffractometer.

3.2. Effect of the DAC on Data Quality

Subsequently, the crystal was placed in the mock-DAC and patterns were recorded. Because of the contributions of the single-crystal diamond peaks, and the powder lines of the steel gasket, an increased background, and an increased signal-to-noise ratio, data-reduction routines that are well established on TOPAZ failed here. In the following, problems encountered and approximations used for the data reduction and analysis are discussed.

3.2.1. Increased Background

While light elements (e.g. C, N, O, F, Ne) cause mainly the emission of an alpha or beta radiation, heavier elements (e.g. Fe and Re) produce high enough gamma radiation if exposed to a neutron beam(Lea, 1912). The Anger cameras as used on SNAP and TOPAZ detect neutrons but are also sensitive to gamma rays. Since steel, beryllium-copper, or rhenium gaskets are most commonly used in DACs, the background is significantly increased if the primary beam hits the gasket.
While it is possible to minimise the gamma ray emission if the primary beam enters the cell through the one of the diamonds, this geometry limits the accessible orientations of the single-crystal for existing cell geometries. Far more orientations can be measured if the primary beam enters the cell through the gasket, inevitably resulting in a significant background increase.

For SNAP, the diffraction patterns for the empty instrument (black), the sample on a vanadium pin (blue), and the fully-assembled DAC are given in figure 2(a).

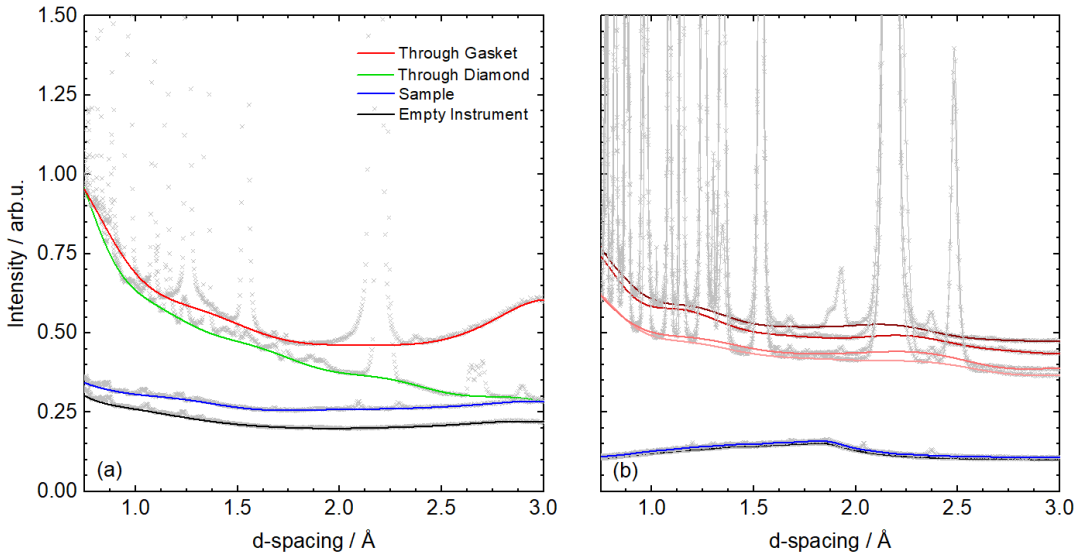

Figure 2. Comparison of background levels on SNAP (a) and TOPAZ (b) for the empty instrument (black), the sample on a vanadium pin (blue), and the full assembled DAC. SNAP: the green curve shows the background in which the primary beam enters the cell through the diamonds only, while the red curve is the background for the case in which the primary beam enters the cell through the gasket. TOPAZ: The four red curves give the background on TOPAZ for various orientations of the cell. All plots are normalised to the proton-current and vanadium-corrected.

All plots are normalised to the proton-current and corrected for instrumental effect by normalising to a measurement of a vanadium standard. The green curve shows the background in which the primary beam enters the cell through the diamonds only, while the red curve is the background for the case in which the primary beam enters the cell through the gasket. Note, that the background level for the high-Q data are of a similar magnitude in both cases; the background increases significantly in the high-Q regime if the gasket is in the primary beam path. For most elements, the absorption cross section σ^a is inversely proportional to the wave vector $k = \frac{2\pi}{\lambda}$. This leads to more neutrons being absorbed at higher wavelengths and hence more gamma rays being emitted(Sears, 1992). In figure 2 (b) the same data are shown for an experiment on TOPAZ and, similar to the experiments carried out on SNAP, an increased background is observed. (The four red curves show the variation of the background levels for four cell orientations.) However, the background does not increase at low-Q to the same extent as on SNAP.
A background reduction could likely be achieved by a reduction of the beam diameter from 3 mm to the actual dimensions of the sample chamber, however, rather high-precision alignment would be required to ensure the sample is fully bathed by the beam.

It should also be noted that He-based tubes are not expected to suffer from the same issue. Evaluation of this is in progress at SNS's CORELLI beamline, but is outside the scope of this paper.

3.2.2. Gasket Contamination

Gaskets for these experiments consist of poly-crystalline steel and add a parasitic signal to the data. Unlike the parasitic Bragg signal from the single crystal diamond - which is well defined in 3D-reciprocal space - powder lines emanating from the metal gasket pollute entire d-spacing ranges on the detector. In figure 3(a), a sample reflection on top of a powder line is shown. Technically, it should be possible to fit the powder-line and subtract the powder-line from the peak. Such an algorithm has not yet been written for MANTID; Here, we hence excluded all sample reflections overlapping with the d-spacing range of gasket-lines. This approximately halved the accessible Q-range for this experiment.

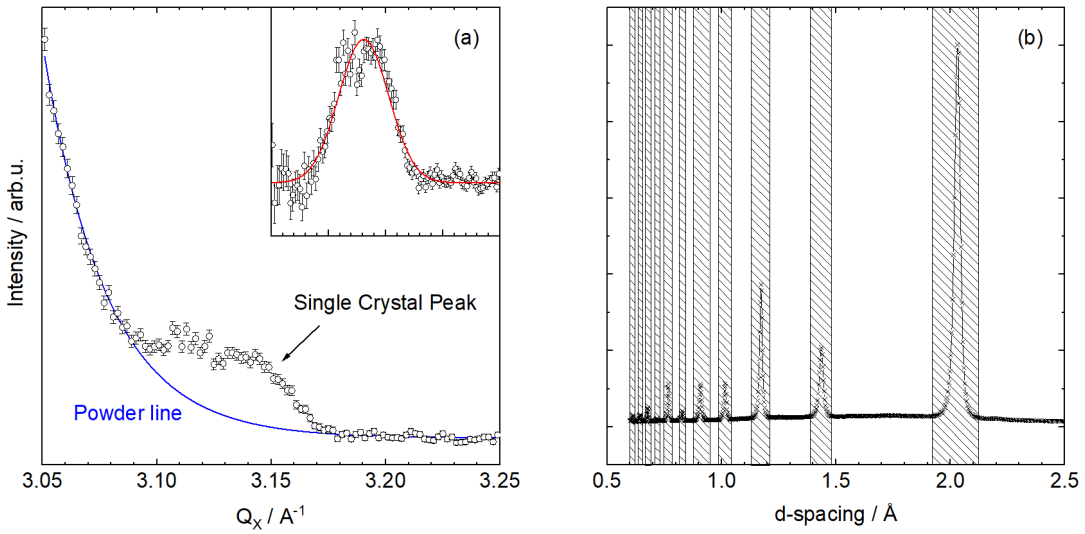

Figure 3. (a) The $31\bar{2}$ single crystal peak of DKDP on top of a powder line caused by the metal gasket of a DAC. The blue curve being gives an exponential fit to the powder line and the insert shows the single crystal peak after the subtraction of the powder line. (b) Integration over the whole detector area after masking all single crystal peaks. The resulting powder lines are caused by the metal gasket (shaded d-spacing regimes); those regions were excluded during the data reduction.

3.2.3. Signal-to-Noise Ratio

While it is not possible to reduce the background with a longer collection time, the signal-to-noise ratio improves with time. As a threshold for the peak integration we chose $I/\sigma = 3$. For the measurement of one orientation, the number of integrable reflections above the s/n ratio doubled with time - after 3, 6, and 8 h the number of integrable reflections were 5-10, 20-30, and >45, respectively.

3.2.4. Attenuation Correction

The sample volume of the DAC-sized crystal was about 0.028 mm^3. In comparison, a metal gasket of a diameter 6.0 mm and a height of 0.5 mm has a volume of 14.137 mm^3 - about 500 times larger. Even if the neutron beam does not illuminate the whole gasket, its illuminated volume exceeds the sample volume. For the attenuation correction, only

the contributions of the steel gasket were taken into consideration. A spherical model was used with the radius of the attenuation sphere chosen to be 1.5 mm - the radius of the beam used for this experiment - and consisted of Fe, Cr and Ni in their respective abundance. (Stainless steel as used for this experiment is an alloy composing of roughly 70% Fe, 20% Cr, and 10% Ni. The other elements in stainless steel such as Mg, Si, P and C were omitted in this model for their abundance is usually less than 2% and the attenuation of these elements is low).

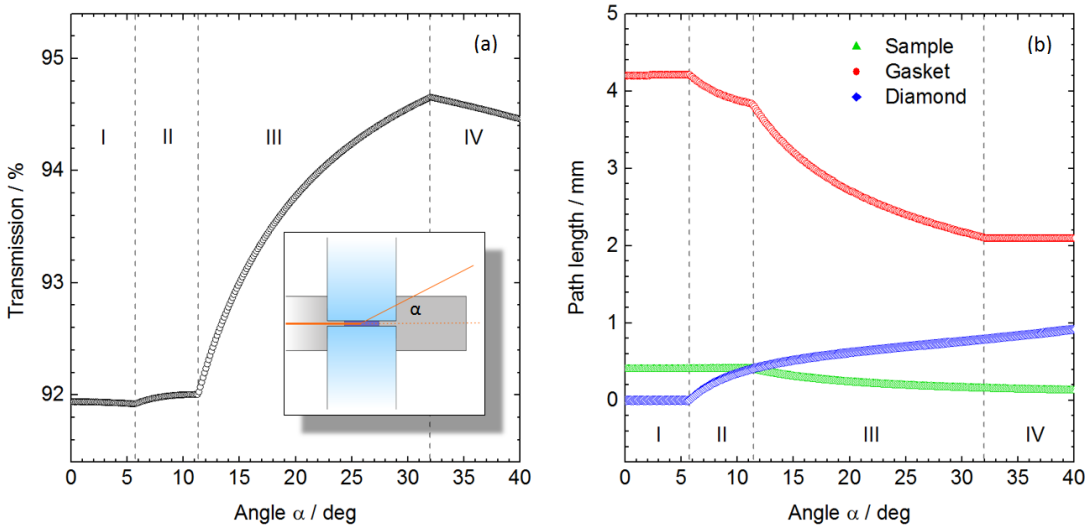

Figure 4. (a) Transmission of a steel gasket for the geometry Φ=-15^o, X=135^o and Ω=0^o. The model of a DAC used for this experiment is shown in the inset. For the beam, four cases for the path can be distinguished: (I) diamond-only, (II) diamond-gasket, (III) gasket-diamond-gasket, and (IV) gasket-only. (b) The respective path lengths through diamond and gasket.

Furthermore, we tried to improve the attenuation model using an analytical beam-tracing approach; To that end, a 3-dimensional model of a diamond anvil cell was created in Python (cf. inset in the left panel of figure 4). This model has the same frame of reference as the TOPAZ instrument and is freely rotatable in 3D about Φ, χ and Ω (cf. TOPAZ specification sheet(Wang et al., 2018)). Instead of a diamond with a pavilion-angle of 49^o (as in a real DAC), we modeled the diamond as a cylinder with the same radius as the culet. This simplification can be justified by two reasons. Firstly, as can be seen in figure 4 (b) the overall path-length through the diamond is small compared to the path-length through the gasket. And secondly, the scattering cross-sections of carbon (σ_s=5.551 barns, σ_a=0.004 barns) relative to those of iron (σ_s=11.62 barns, σ_a=2.56 barns), chromium (σ_s=3.49 barns, σ_a=3.05 barns), and nickle (σ_s=18.50 barns, σ_a=4.49 barns) results in a smaller contribution of diamond to the total attenuation(Sears, 1992).
The total beam-path $D_i = d_i^{in} + d_i^{out}$ was calculated, with d^{in} and d^{out} being the path lengths through the respective materials to the centre of the sample chamber and from the centre out of the cell, respectively. The un-attenuated intensities, I_0, can then be calculated according to Beer's law from the observed intensities, I_{obs} as

$$I_{obs} = I_0 \cdot \prod_{i=1}^{n} \exp\left(-\rho_i D_i \sigma_i^s - \rho_i D_i \sigma_i^{a,\ddagger} \cdot \frac{m_{neut}\lambda}{h} \cdot 2200\frac{m}{s}\right). \quad (1)$$

In this equation ρ_i are the atom densities in atoms/m^3, D_i are the path-lengths, σ_i^s are the scattering cross-section and $\sigma_i^{a,\ddagger}$ are the absorption cross-section at 1.798 Å (v=2200 m/s); see Sears (1992) and Giacovazzo et al. (1992). For most nuclides, the scattering lengths and cross-sections are independent of the incident neutron wave vector in the thermal neutron region, while the absorption cross-sections are inversely proportional to v, the velocity of the neutron (Koester, 1977; Sears, 1992).

The calculated transmission as a function of the angle α (the angle of a beam relative to the gasket plane) for the geometry Φ=-15^o, X=135^o and Ω=0^o is given in figure 4. It can be seen that the intensities of the reflected beam in this case vary by about 3%, with beams that are in plane with the gasket being attenuated strongest. This model, although more accurate than the spherical model, did not improve the R_w for the refinements significantly.
An attempt to refine anisotropic thermal parameters was made but proved unstable because the number of observed reflections was insufficient.

In a TOF neutron diffraction experiment, where the incident neutron beam travels through a single-crystalline diamond, neutrons with certain wavelengths will fulfill the Bragg condition and and hence be scattered. This can be seen in the transmission spectrum by 'diamond dips', which further decreases the intensity of incident neutrons around certain wavelengths (Guthrie, M. and Pruteanu, C. and Donnelly M-E. and Molaison J. J. and dos Santos, A. M. and Loveday, J. S. and Boehler, R. and Tulk, C. A., 2017).Loveday, McMahon, and Nelmes (1990) showed that this effect is negligible at low pressures but becomes much more pronounced with pressure. Since experiments in this work were a) carried out in a way that the primary beam enters the cell through the gasket and b) were not carried out at high enough pressures, this effect was ignored in this work. At higher pressures and other geometries, an additional correction for "diamond dips" also has to be applied.

3.2.5. Extinction Correction

For the extinction correction a first-order Lorenzian model from GSAS-I was used. A better result for the bare crystal was obtained using the extinction models by Becker and Coppens 1974 (Becker & Coppens, 1974) as employed by the Jana software package, but was not used here since all other error sources for this experiment outweighed the error due to extinction.

3.2.6. Integration and Refinements

Several routines for the integration of the Bragg reflections obtained from the experiment were investigated. In figures 5 and 6, the plots show the calculated vs the observed structure factors, F_{calc} and F_{obs}, respectively, for the investigated integration and data-reduction routines. In an ideal case, F_{calc} from the structural model and F_{obs} obtained from the experiment will agree within the statistical error of the measurement, F_{calc}=F_{obs}, indicated by the broken grey line. The insets in the respective plots show the relative difference between F_{obs} and F_{calc} ($|F_{obs} - F_{calc}|/F_{obs}$) as a function of F_{obs}.

First, the integrations were carried out using the standard TOPAZ algorithm (DAC_a), which automatically predicts peaks, finds an orientation matrix (UB-matrix,

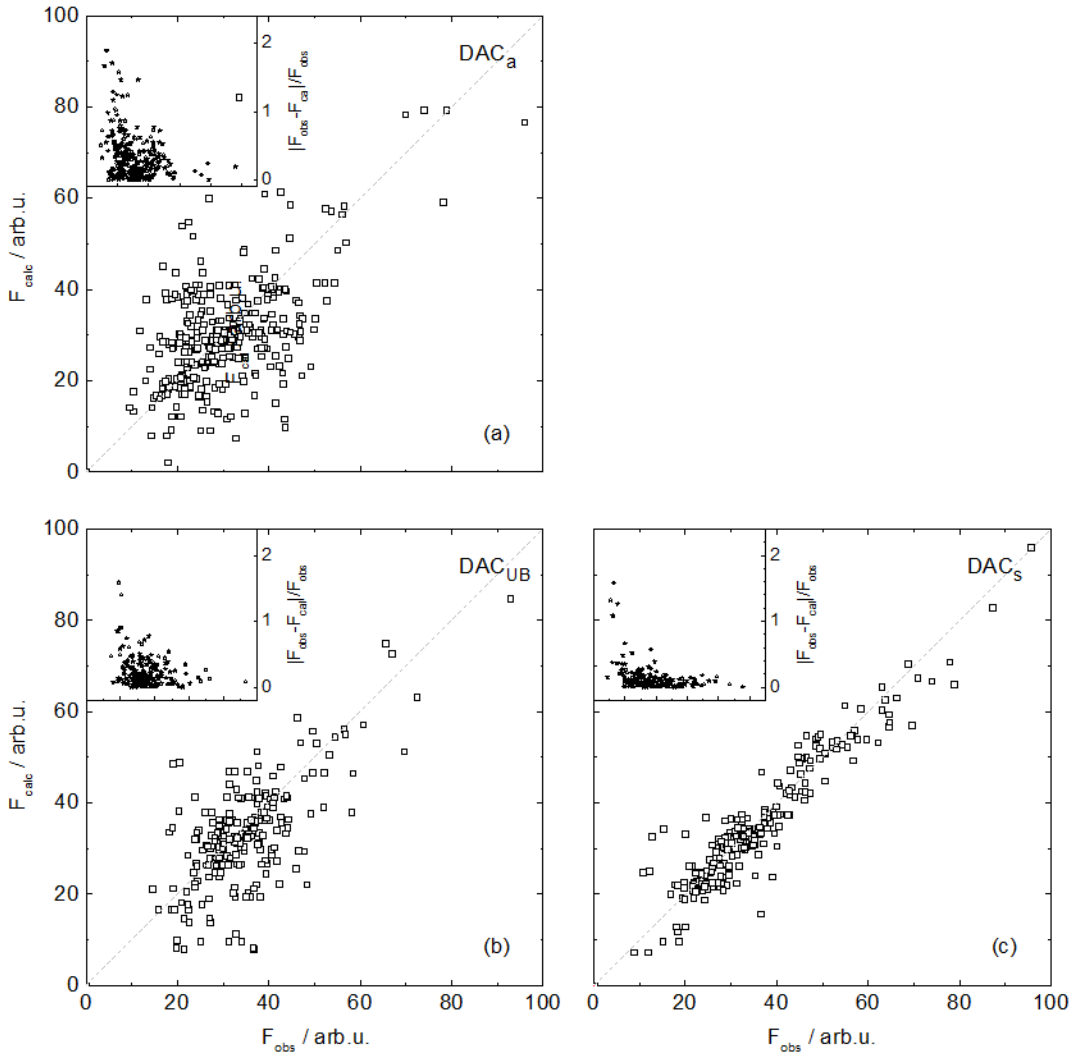

Figure 5. Observed versus calculated structure-factors for: (a) using the standard TOPAZ algorithm (DAC_a), (b) a refined UB for every orientation (DAC_{UB}), and (c) a selected subset of peaks (DAC_s). The insets give the relative difference between observed and calculated structure-factors as $|F_{obs} - F_{calc}|/F_{obs}$ as a function of F_{obs}.

see Busing and Levy (1967)), and integrates the respective peaks. This automated algorithm failed here, as can be seen by strong scattered structure factors in figure 5 (a). It is not surprising, that small structure factors (usually high-Q structure factors) fit particularly poorly. This refinement gave an overall R_w of 0.201, with R_w being the residual factor (R-factor)

$$R_w = \frac{\sum ||F_{obs}| - |F_{calc}||}{\sum |F_{obs}|}. \tag{2}$$

With a refined UB-matrix for every orientation (DAC_{UB}), R_w was reduced to 0.145, suggesting still a bad fit of the model to the data. Hence we picked the peaks manually in order to ensure that the Bragg reflections actually used for the refinement were not

overlapped by a powder line or close to a detector edge, and had a sufficient s/n-ratio for the integration. Using this subset of peaks (DAC_S), we obtained an R_w of 0.117, a much better result than for the other routines. The F_{obs} vs F_{calc} plots for the DAC_{UB} and DAC_S routine are depicted in figures 5 (b) and (c), respectively. The integration discussed above were carried out using the *IntegrateEllipsoids* MANTID-algorithm (see MANTID documentation and Schultz et al. (2014)).

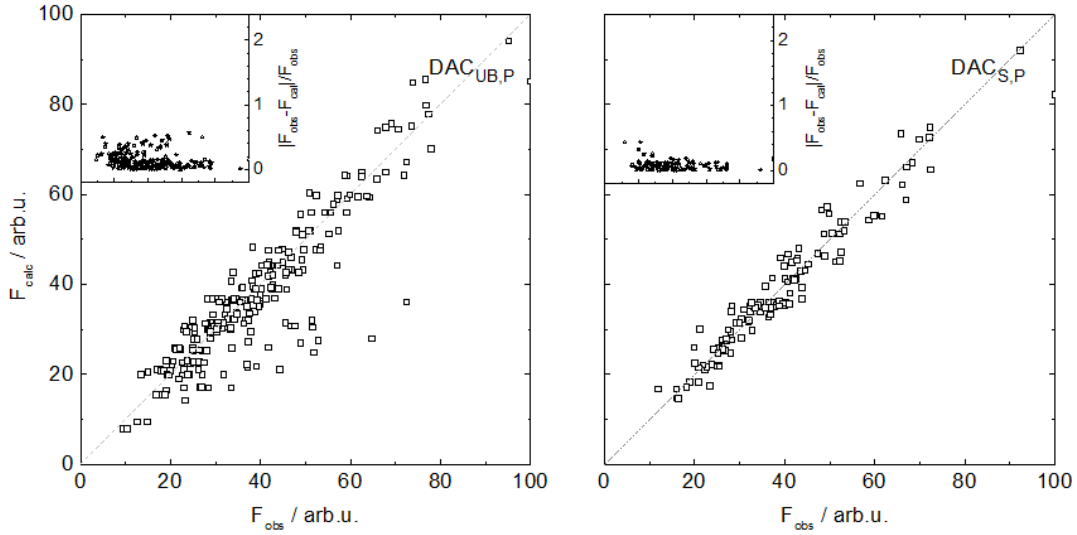

Figure 6. Observed vs Calculated Structure factors for (d) a refined UB for every orientation ($DAC_{UB,P}$), and (e) a selected subset of peaks ($DAC_{S,P}$). The integrations were carried out using the *IntegratePeaksProfileFitting* algorithm. The insets give the relative difference between observed and calculated structur facors as $|F_{obs} - F_{calc}|/F_{obs}$ as a function of F_{obs}.

The same data sets as used in DAC_{UB} and DAC_S were then re-integrated using the *IntegratePeaksProfileFitting* algorithm ($DAC_{UB,P}$ and $DAC_{S,P}$, respecively). This algorithm uses two Gaussians to fit a peak in Q-space, an actual fitting technique. Compared to the *IntegrateEllipsoids* algorithm, the intensities and sigmas of the fitted peaks are in a better agreement with the data, particularly for weak reflections close to the s/n threshold (see MANTID documentation and Schultz et al. (2014)). The best fit of the data to the model was obtained using this method (cf. figure 6) with R_w of 0.110 and 0.087, respectively.
The respective results for all the refinements are given in table 4 in the appendix. Furthermore, all structural parameters are within 1σ of the data obtained from the bare crystal and hence comparable. Note that the data set integrated using the *IntegratePeaksProfileFitting* is not only more accurate than the data from the other routines, it also is 2-3 times more precise. Full structural refinements from single-crystal data in DACs are therefore possible on well-calibrated diffractometers with Anger cameras.

3.3. Is Quantitative Structure Refinement of Hydrogen-Rich Systems in a DAC on SNAP Feasible?

SNAP has a much higher flux than TOPAZ, a feature that is needed for high-pressure experiments. However, fully quantitative SXL work on systems containing light elements has not been explored yet - hence its capabilities for single-crystal diffraction

had to be tested. To that end, a single crystal of about 1 mm^3 was placed on a vanadium pin and and diffraction patterns of ten orientations, each measured for 3 h, were collected. Compared to TOPAZ, the detector coverage is more limited and the sample stage deployed for this experiment allowed for rotations about the vertical omega axis only. These limitations significantly reduce the accessible reflections in comparison to TOPAZ. We were able to utilise TOPAZ data-reduction procedures for SNAP.
The results of the refinements for the data collected are given in table 5 (cf. table 5 appendix). A total of 1027 reflections were observed and an R_w of 0.067 was obtained. All structural parameters are within 1σ of the reference measurement carried out on TOPAZ (see section 3.1). Note that the lattice parameters in the DAC experiment deviates from the lattice parameter obtained from the bare crystal. This deviation stems from the limited rotation geometry which leads to an under-representation of reflections along the c-axis, and from a broad profile of the sample reflections in this experiment which introduced an error in the calculation of the orientation matrix. While the former is an intrinsic problem of the instrument, the latter was caused by a beam-guide with a suboptimal curvature. The accuracy of the determined lattice parameters greatly improved after an upgrade of the guide in 2018 (see lattice parameters for ice VI in section 3.4. which were determined after the guide-upgrade).

The same experiment as detailed above for TOPAZ was repeated with a DAC-sized crystal and similar results for the refinement were obtained (cf. table 5). A total of 279 reflections were observed and an R_w of 0.090 obtained. Even though the number of observed reflections dropped by a factor of 4, the structural parameters remained well within 1σ of the larger crystal and within 1-2σ of the reference measurement on TOPAZ. Please note that the error-bars only tripled by reducing the volume by a factor of 35 from 1.028 mm^3 to 0.028 mm^3.
These results show that SNAP as it is setup presents some limitations but in principle similar data quality as on TOPAZ can be achieved and as such can yield accurate structural data.

Finally, the smaller crystal was placed in a real neutron DAC and measured as well. The set-up allows for rotation about ω only with the primary beam entering the cell through the gasket. The DAC was rotated about ω to six orientations and patterns were collected for 3 h each. Despite the short collection time, 56 Bragg peaks with an acceptable I/σ ratio were found and integrated. The empirical $3n$-rule suggests that for a (isotropic) refinement of DKDP (4 atoms) at least 48 reflections are needed - which was achieved here.

Lattice parameters, and structural parameters of this experiment are shown in table 5. The fractional refinements carried out on with this small data set resulted in an overall R_w of 0.336. The atomic coordinates obtained from this data set are still correct, but due to the the reciprocal space coverage explored, the uncertainties are very large and in the order of 0.05-0.20. With a similar collection time as on TOPAZ (6-8 h), better results should be possible.

Table 1. Comparison of structural parameters of ice VI as reported by Kuhs *et al.* (Kuhs et al., 1984) (top) and this study (bottom). Data were collected on SNAP.

	x	y	z	Occ.	U_{iso}
O1 (2a)	0.7500(00)	0.2500(00)	0.7500(00)	1	0.0299(49)
O2 (8g)	0.7500(00)	0.5295(43)	0.1339(38)	1	-
D1 (8g)	0.7500(00)	0.4628(92)	-0.0131(86)	0.5	0.0380(51)
D2 (8g)	0.7500(00)	0.3103(64)	-0.1365(101)	0.5	-
D3 (8g)	0.7500(00)	0.6812(10)	0.1248(18)	0.5	-
D4 (16h)	0.1325(41)	0.5301(51)	0.1844(51)	0.5	-
O1 (2a)	0.7500(00)	0.2500(00)	0.7500(00)	1	0.0208(25)
O2 (8g)	0.7500(00)	0.5337(25)	0.1306(23)	1	-
D1 (8g)	0.7500(00)	0.4450(40)	-0.0120(50)	0.5	0.0211(27)
D2 (8g)	0.7500(00)	0.3850(60)	-0.1423(29)	0.5	-
D3 (8g)	0.7500(00)	0.6799(32)	0.1330(40)	0.5	-
D4 (16h)	0.1333(27)	0.5330(30)	0.7930(25)	0.5	-

3.4. Application on Samples Under Pressure: A Structural Study of Ice VI

In order to test our method against a sample under pressure, a single crystal of ice VI was measured. The sample was grown under a pressure of 1.1 GPa in a DAC ($\varnothing_{culet}$=1.43 mm; steel gasket, $\varnothing_{hole}$=800 μm, indented to 136 μm; pressure from the EOS of ice VI as given by Bezacier et al. (2014)) by repeatedly melting and re-crystallising an ice VI powder resulting in the formation of a single-crystal. The cell containing the sample was then aligned on the SNAP instrument and patterns for three orientations were collected (about 12h per orientation). Altogether, 84 structure factors were obtained after the data reduction procedure and outlier removal. From the UB-matrices, the lattice parameters of the single-crystal were found to be a=b=6.205(6)Å and c=5.709(2)Å.

Similarly to DKDP, ice VI is a well known structure and has been studied thoroughly (Bezacier et al., 2014; Bridgman, 1912; Kuhs, Ahsbahs, Londono, & Finney, 1989; Kuhs et al., 1984; Kuo & Kuhs, 2006). Ice VI shows a tetragonal crystal system with the space group $P4_2/nmc$; its unit cell contains 10 water molecules and has the dimensions a=6.1845(1)Å and c=5.6981(1)Å at 1.26 GPa (Bezacier et al., 2014). The oxygen atoms are on a 2a and 8g site, and the hydrogens are located on three 8g sites and one 16h site - hence, only 17 parameters are needed for a structural refinement with isotropic atomic displacement parameters.

A preliminary refinement for the 17 parameters in an ice VI crystal resulted in an overall weighted R-factor of R_w= 0.1302; constraining the isotropic atomic displacement parameters for the two atoms dropped the R_w further to 0.1109. (Similar to the DKDP a refinement with anisotropic thermal parameters was attempted but gave no physically sensible results.)
The structural parameters for ice VI as given by Kuhs et al. (1984) and the values for this refinement are shown in table 1.

4. Conclusion

We performed several neutron-scattering experiments on the TOPAZ and SNAP beam lines at the Spallation Neutron Source (SNS) at Oak Ridge National Laboratory (ORNL). As a samples, we used deuterated potassium dihydrogen-phasphate

Table 2. Summary of the refinements for the crystals and the crystal in a DAC-sample environment for SNAP and TOPAZ, respectively. The collection time per orientation is give as well as the number of reflections after outlyer removal. Only best refinements are shown - for detailed information see tables 4 and 5 in appendix.

Crystal	Small	Large	Small	DAC	DAC	DAC
Sample	DKDP	DKDP	DKDP	DKDP	DKDP	Ice VI
Instrument	TOPAZ	SNAP	SNAP	TOPAZ	SNAP	SNAP
Orientations	10	6	6	10	6	3
Collection time	3 h	3 h	3 h	6-8 h	3 h	12 h
Reflections	1044	1027	279	167	56	84
R_w	0.045	0.067	0.090	0.087	0.336	0.1302

(DKDP) and water ice VI. Results of our suite of experiments on single-crystal neutron-diffraction in diamond anvile cells promising results that are summarised in table 2.

In a first trial experiment we showed that it is possible to obtain data of high quality from a DAC-sized crystal. Our results are in good accordance with the crystal structure published by Tibballs and Nelmes (1982), indicating that it is feasible to reduce the sample size to a volume smaller than that of a typical netron-DAC cavity. We repeated the experiment in the sample environment of a diamond anvil cell. Despite the - not surprising - loss of data quality, we were able to obtain enough structure factors to refine the structure with the same accuracy as in the case of the bare crystal, however, the errors on the structural parameters increased significantly.

In a second step, we bench-marked SNAP, an instrument primarily used for powder diffraction, for quantitative analysis of single crystal data. We were able to show that quantitative single crystal diffraction on hydrogen-rich materials on SNAP is possible and that the data is of similar quality to TOPAZ. Subsequently, we collected patterns of a DAC-sized sample to test the volume limitations of SNAP. We were able obtain 279 structure factors - enough to refine the structure to R_w=0.090.

Finally, we collected patterns of a single crystal samples of DKPD and ice in a diamond anvil cell on SNAP. Due to time restrictions, we only obtained 56 reflection from 6 orientations measured for 3 h each; a similar experiment carried out on TOPAZ (10 orientations for 6-8 h each) in comparison resulted in about 300 structure factors. Nevertheless was it possible to refine the structure from the obtained data, however, the large errors on the atomic coordinates suggest that a similar collection time as on TOPAZ is needed for precise results.

The data reduction procedure was then tested against a crystal of ice VI which was grown in a DAC. Diffraction patterns of three orientations (measured for 12h each) resulted in 84 observed structure factors - enough to carry out a refinement that reproduced the published structure of ice VI, proving that quantitative HP-SCND on SNAP in a DAC is possible.

Acknowledgement(s)

This work was conducted at the Spallation Neutron Source (SNS), a Department of Energy (DoE) user facility BM, JJM, XW, AMS, MG and JSL conducted the experiments. BM analysed the data. LDD synthesized the samples. BH and RB contributed to the context of pressure experimentation. All authors contributed to discussions of the work, analysis and to the writing of the manuscript. We would like to thank Vickie E. Lynch for discussion and advice regarding MANTID.
BM acknowledges funding under SUPA's PECRE scheme, by the Shull Wollan center at ORNL and by the ESF through the Hecate grant.

Disclosure statement

References

Arnold, O., Bilheuxc, J. C., Borreguero, J. M., Buts, A., Campbell, J. I., Chapon, L., ... Zikovsky, J. (2014). Mantid—Data analysis and visualization package for neutron scattering and μSR experiments. *Nuclear Instruments and Methods in Physics Research Section A*, *764*, 156-166.

Becker, P. J., & Coppens, P. (1974). Extinction within the Limit of Validity of the Darwin Transfer Equations - General Formalisms for Primary and Secondary Extinction and Their Application to Spherical Crystals. *Acta Cryst.*, *A30*(129), 129–147.

Besson, J., Nelmes, R., Hamel, G., J.S.Loveday, Weill, G., & S.Hulld. (1992). Neutron powder diffraction above 10 GPa. *American Mineralogist*(907), 180–181.

Bezacier, L., Journaux, B., Perrillat, J. P., Cardon, H., Hanfland, M., & Daniel, I. (2014). Equations of state of ice VI and ice VII at high pressure and high temperature. *Journal of Chemical Physics*, *141*(10). Retrieved from `http://dx.doi.org/10.1063/1.4894421`

Bezacier, L., Tobie, G., Bollengier, O., Grasset, O., Menn, E. L., & Oancea, A. (2013). Dissociation temperatures of methane hydrates at high pressure : Implications for the differentiation of Titan's interior. , *6*(259285), 6–7.

Binns, J., Kamenev, K. V., McIntyre, G. J., Moggach, S. A., & Parsons, S. (2016). Use of a miniature diamond-anvil cell in high-pressure single-crystal neutron Laue diffraction. *IUCrJ*, *3*, 168–179.

Boehler, R., Guthrie, M., Molaison, J. J., Santos, A. M., Sinogeikin, S., Pradhan, N., & Tulk, C. A. (2013). Large-volume diamond cells for neutron diffraction above 90 GPa. *High Pressure Research*, *33*, 546–554.

Bridgman, P. W. (1912). Water, in the Liquid and Five Solid Forms, under Pressure. *Proceedings of the American Academy of Arts and Sciences*, *47*(13), 441–558.

Busing, W. R., & Levy, H. A. (1967). Angle calculations for 3- and 4-circle X-ray and neutron diffractometers. *Acta Crystallographica*, *22*(4), 457–464.

Calder, S., An, K., Boehler, R., Dela Cruz, C. R., Frontzek, M. D., Guthrie, M., ... Tucker, M. G. (2018). A suite-level review of the neutron powder diffraction instruments at Oak Ridge National Laboratory. *Review of Scientific Instruments*, *89*(9).

Cavazzoni, C., Chiarotti, G. L., Scandolo, S., Tosatti, E., Bernasconi, M., & Parrinello, M. (1999). Superionic and Metallic States of Water and Ammonia at Giant Planet Conditions. *Science*, *283*, 44-46.

Chen, X., Struzhkin, V., Yu, Y., Goncharov, A. F., Lin, C., Mao, H., & Hemley, R. J. (2010). Enhancement of superconductivity by pressure-driven competition in electronic order. *Nature*, *466*(7309), 950–953.

Cui, L., Chen, N. H., & Silvera, I. F. (1995). Excitations, order parameters, and phase diagram of solid deuterium at megabar pressures. *Physical Review B*, *51*(21), 14987–14997.

Drozdov, A. P., Eremets, M. I., Troyan, I. A., Ksenofontov, V., & Shylin, S. I. (2015). Conventional Superconductivity at 203 Kelvin at High Pressures in the Sulfur Hydride system. *Nature*.

Duang, D., Liu, Y., Tian, F., Li, D., Huang, X., Zhao, Z., ... Cui, T. (2014). Pressure-induced Metallization of Dense $(H_2S)_2H_2$ with High-T_c Superconductivity. *Scientific Reports*, *4*(6968), 30–32.

Gao, L., Xue, Y., Chen, F., Xiong, Q., Meng, R. L., Ramirez, D., ... Mao, H. K. (1994). Superconductivity up to 164 K in $HgBa_2Ca_{m-1}Cu_mO_{2m+2+\delta}$ (m=1, 2, and 3) under quasi-hydrostatic pressures. *Physical Review B*, *50*(6), 4260–4263.

Geneste, G., Torrent, M., & Loubeyre, P. (2012). Strong Isotopic Effect in Phase II of Dense Solid Hydrogen and Deuterium. (phase II).

Giacovazzo, C., Monaco, H., Viterbo, D., Scordari, F., Gillli, G., Zanotti, G., & Catti, M. (1992). *Fundamentals of Crystallography* (Vol. 2).

Goncharenko, I., & Loubeyre, P. (2005, 07). Neutron and x-ray diffraction study of the broken symmetry phase transition in solid deuterium. *Nature*, *435*, 1206-9.

Grzechnik, A., Meven, M., & Friese, K. (2018). Single-crystal neutron diffraction in diamond anvil cells with hot neutrons research papers. (2016), 351–356.

Guillot, T. (2005). The Interior of Gas Planets : Models and Outstanding Questions. *Annu. Rev. Earth Planet. Sci.*, *33*, 493–530.

Guthrie, M., Boehler, R., Molaison, J. J., Haberl, B., dos Santos, A. M., & Tulk, C. (2019, 5). Structure and disorder in ice VII on the approach to hydrogen-bond symmetrization. *Physical Review B*, *99*(18).

Guthrie, M. and Pruteanu, C. and Donnelly M-E. and Molaison J. J. and dos Santos, A. M. and Loveday, J. S. and Boehler, R. and Tulk, C. A. (2017). Radiation attenuation by single-crystal diamond windows. *J. App. Cryst.*, *50*(1), 76-86.

Haberl, B., Dissanayake, S., Wu, Y., Myles, D. A., Dos Santos, A. M., Loguillo, M., ... Boehler, R. (2018). Next-generation diamond cell and applications to single-crystal neutron diffraction. *Review of Scientific Instruments*, *89*(9).

Haberl, B., Dissanayake, S., Ye, F., Daemen, L. L., Cheng, Y., Li, C. W., ... Boehler, R. (2017). Wide-angle diamond cell for neutron scattering. *High Pressure Research*, *37*(4), 495–506.

Helled, R., Anderson, J. D., Podolak, M., & Schubert, G. (2011). Interior models of uranus and neptune. *Astrophys. J.*, *15*.

Hubbard, W. B. (1997). Neptune's Deep Chemistry. *Science*, *275*, 1279-1280.

Klotz, S. (2013). *Techniques in High Pressure in Neutron Scattering* (1st ed.). Boca Raton: CRC Press.

Koester, L. (1977). *Neutron physics* (Vol. 1). Springer.

Kuhs, W. F., Ahsbahs, H., Londono, D., & Finney, J. L. (1989). In-situ crystal growth and neutron four-circle diffractometry under high pressure. *Physica B: Condensed Matter*, *156-157*, 684–687.

Kuhs, W. F., Finney, J. L., Vettier, C., & Bliss, D. V. (1984). Structure and hydrogen ordering in ices VI , VII , and VIII by neutron powder diffraction. , *3612*(81), 3612–3623.

Kuo, J. L., & Kuhs, W. F. (2006). A first principles study on the structure of ice-vi: Static

distortion, molecular geometry, and proton ordering. *Journal of Physical Chemistry B*, *110*(8), 3697–3703.

Larson, A., & Dreele, R. V. (2000). GSAS Manual. *Los Alamos National Laboratory Report, LAUR*, 86-748.

Lea, D. E. (1912). Secondary Gamma Rays Excited by the Passage of Neutrons through Matter. *Proceedings of the Royal Society of London. Series A*, *150*(13), 637–668.

Loveday, J. S., McMahon, M. I., & Nelmes, R. J. (1990). The effect of diffraction by the diamonds of a diamond-anvil cell on single-crystal sample intensities. *Journal of Applied Crystallography*, *23*(5), 392–396.

Loveday, J. S., & Nelmes, R. J. (2003). High-pressure neutron diffraction and models of titan. *High Pressure Research*, *7959*.

Mao, H.-k., & Hemley, R. (2001). Ultrahigh transitions in solid hydrogen. *Reviews of Modern Physics*, *66*(2), 671–692.

Millot, M., Hamel, S., Rygg, J., Celliers, P. M., Collins, G. W., Coppari, F., ... Eggert, J. H. (2018). Experimental evidence for superionic water ice using shock compression. *Nat. Phys.*(14), 297–302.

Pauling, L. (1935). The Structure and Entropy of Ice and of Other Crystals with Some Randomness of Atomic Arrangement. *Journal of the American Chemical Society*, *57*(12), 2680-2684.

R. Boehler *et al.* (2017). Novel diamond cells for neutron diffraction using multi-carat CVD anvils. *Rev. Sci. Inst.*(88), 08390.

Schultz, A. J., Jørgensen, M. R. V., Wang, X., Mikkelson, R. L., Mikkelson, D. J., Lynch, V. E., ... Hoffmann, C. M. (2014). Integration of neutron time-of-flight single-crystal Bragg peaks in reciprocal space. *Journal of Applied Crystallography*, *47*(3), 915–921.

Sears, V. F. (1992). Neutron scattering lengths and cross sections Special Feature Neutron scattering lengths and cross sections. *Neutron News*, *3*(3), 26–37.

Shin, K., Kumar, R., Udachin, K. A., Alavi, S., & Ripmeester, J. A. (2012). Ammonia clathrate hydrates as new solid phases for Titan, Enceladus, and other planetary systems. *Proceedings of the National Academy of Sciences*, *109*(37), 14785–14790.

Silvera, I. F. (1980). The solid molecular hydrogens in the condensed phase: Fundamentals and static properties. *Rieview of Modern Physics*, *52*(2), 393–452.

et al., J. M. B. (2002). *Biochemistry* (5th ed.). Oxford, New York: W.H. Freeman.

Tibballs, J. E., & Nelmes, R. J. (1982). The P-T dependence of the crystal-structure of KDP and DKDP above T_c. *J. Phys. C: Solid State Phys.*, *15*(25), L849–L853.

Tobie, G., Grasset, O., Lunine, J. I., Mocquet, A., & Sotin, C. (2005). Titan ' s internal structure inferred from a coupled thermal-orbital model. *Icarus*, *175*, 496–502.

Toby, B. H. (2001). EXPGUI, a graphical user interface for GSAS. *J. Appl. Cryst.*(34), 210-213.

Wang, X., Hoffmann, C., & dos Santos, A. (2018). *TOPAZ - Single crystal Diffractometer.* Retrieved 2019-26-07, from `https://neutrons.ornl.gov/sites/default/files/TOPAZ.pdf`

Wollan, E. O., Davidson, W. L., & Shull, C. G. (1949). Neutron Diffraction Study of the Structure of Ice. , *822*(9).

Table 3. Orientations of the DKDP crystal. The respective goniometer angles X, Φ, and Ω in degree are given. Note that on TOPAZ X is fixed to 135°, and on SNAP X and Φ are fixed to 0°

Sample	DKDP			DKDP			DKDP		
Size	Small			Small (DAC)			Large		
Diffractometer	TOPAZ			TOPAZ			SNAP		
Orientation	X / deg	Φ / deg	Ω / deg	X / deg	Φ / deg	Ω / deg	X / deg	Φ / deg	Ω / deg
1	135.00	0.02	0.00	135.00	-15.00	-0.02	0.00	0.00	129.98
2	135.00	-26.70	105.95	135.00	-15.00	29.99	0.00	0.00	149.96
3	135.00	28.71	-149.95	135.00	-15.00	-30.01	0.00	0.00	169.96
4	135.00	-177.09	-174.68	135.00	20.00	-25.00	0.00	0.00	189.96
5	135.00	-51.33	10.75	135.00	20.00	25.02	0.00	0.00	209.95
6	135.00	116.75	10.14	135.00	55.00	20.03	0.00	0.00	229.96
7	135.00	44.88	31.08	135.00	55.00	80.02	0.00	0.00	249.96
8	135.00	-130.16	14.12	135.00	55.00	43.99	0.00	0.00	269.96
9	135.00	52.44	140.49	135.00	55.00	69.01	0.00	0.00	289.96
10	135.00	14.35	100.26	135.00	40.00	47.00	0.00	0.00	299.96

Sample	DKDP			DKDP		
Size	Small			Small (DAC)		
Diffractometer	SNAP			SNAP		
Orientation	X / deg	Φ / deg	Ω / deg	X / deg	Φ / deg	Ω / deg
1	0.00	0.00	64.97	0.00	0.00	-60.02
2	0.00	0.00	79.98	0.00	0.00	-74.98
3	0.00	0.00	94.96	0.00	0.00	-89.96
4	0.00	0.00	109.96	0.00	0.00	-104.96
5	0.00	0.00	124.96	0.00	0.00	-119.96
6	0.00	0.00	139.96	0.00	0.00	-134.96

Table 4. Comparison of refinements of data of DKDP in a diamond anvil cell (V=0.028 mm^3). The data was integrated using the standard TOPAZ algorithm (DAC_a), a refined UB for every orientation (DAC_{UB}), and a selected subset of peaks (DAC_s) to exclude peaks on powder lines. While for the first integrations were carried out using the *IntegrateEllipsoid* algorithm, the last column (DAC_p) was treated as the DAC_s data but integrated using the *IntegratePeaksProfileFitting* algorithm. The well established routine for bare crystals as used on TOPAZ is labelled *Auto*.

Crystal	KDP*	DKDP*	DKDP	DKDP	DKDP	DKDP	DKDP	DKDP
Sample Environment	None	None	None	DAC	DAC	DAC	DAC	DAC
Int. Method			Auto	DAC_a	DAC_{UB}	DAC_S	$DAC_{UB,P}$	$DAC_{S,P}$
Note	Nelmes '82	Nelmes '82						
Obs	-	-	1044	359	216	222	323	167
Rw(Fobs)	0.022	0.055	0.045	0.201	0.145	0.117	0.110	0.087
a	7.4521(4)	7.4645(3)	7.4505(12)	7.4534(10)	7.4534(4)	7.4660(7)	7.4713(3)	7.4652(8)
c	6.974(2)	6.9678(4)	6.9679(15)	6.9701(8)	6.9732(4)	6.9733(6)	6.9722(2)	6.9779(7)
a/c	0.936	0.934	0.933	0.935	0.936	0.934	0.933	0.934
O-O	2.4944(5)	2.5286(4)	2.5322(4)	2.37(2)	2.3923(4)	2.51(2)	2.507(9)	2.511(9)
O-P	1.5402(4)	1.54207(19)	1.53717(16)	1.51(1)	1.59568(16)	1.551(10)	1.545(4)	1.541(7)
O-D	1.0657(12)	1.0419(3)	1.062(8)	1.13(9)	0.97830(14)	1.071(11)	1.05(1)	1.05(1)
D-D	0.367(3)	0.4511(4)	0.420(16)	0.31(8)	0.44359(6)	0.404(6)	0.45(2)	0.42(6)
x(D)	0.14757(12)	0.14861(2)	0.14844(23)	0.1331(21)	0.1444(18)	0.1528(23)	0.1467(10)	0.1474(18)
y(D)	0.22559(15)	0.22011(2)	0.2217(10)	0.258(11)	0.2204(11)	0.2250(40)	0.2222(12)	0.2220(35)
z(D)	0.12161(47)	0.12041(3)	0.1196(10)	0.146(6)	0.12173(6)	0.1140(40)	0.1229(14)	0.1250(40)
x(O)	0.14839(3)	0.14888(1)	0.14891(11)	0.1438(17)	0.15215(14)	0.1472(15)	0.1494(5)	0.1486(9)
y(O)	0.08264(3)	0.08073(1)	0.08070(11)	0.0909(13)	0.08957(12)	0.0836(12)	0.0822(6)	0.0818(11)
z(O)	0.12584(5)	0.12643(2)	0.12566(11)	0.1166(9)	0.12942(8)	0.1299(21)	0.1254(4)	0.1258(8)
UISO (D)	-	-	0.0279(8)	-0.017(6)	0.17(6)	0.0288(16)	0.0256(16)	0.033(4)
USIO (O)	-	-	0.0183(12)	0.045(9)	0.064(26)	0.0179(21)	0.0146(8)	0.0166(20)

Table 5. Sequentially deteriorating data quality with the crystal size (large about 1 mm^3; small about 0.028 mm^3) and the complexity of the sample environment.

Crystal	KDP*	DKDP*	DKDP (s)	DKDP (l)	DKDP (s)	DKDP (s)
Diffractometer			TOPAZ	SNAP	SNAP	SNAP
Sample Environment	None	None	None	None	None	DAC
Int. Method			Auto	Auto	Auto	DAC_m
Note	Nelmes '82	Nelmes '82				
Obs	-	-	1044	1027	279	56
Rw(Fobs)	0.022	0.055	0.045	0.067	0.090	0.336
a	7.4521(4)	7.469(1)	7.4505(12)	7.4871(7)	7.4871(7)	7.486(3)
c	6.974(2)	6.976(1)	6.9679(15)	7.0025(8)	6.9909(8)	7.002(10)
a/c	0.936	0.934	0.933	0.934	0.934	0.936
O-O	2.4944(5)	2.5286(4)	2.5322(4)	2.535(3)	2.530(8)	2.42(8)
O-P	1.5402(4)	1.54207(19)	1.53717(16)	1.5478(12)	1.544(4)	1.61(5)
O-D	1.0657(12)	1.0419(3)	1.062(8)	1.056(3)	1.066(8)	0.99(12)
D-D	0.367(3)	0.4511(4)	0.420(16)	0.430(5)	0.404(13)	0.5(3)
x(D)	0.14757(12)	0.14861(2)	0.14844(23)	0.14868(24)	0.1487(10)	0.142(14)
y(D)	0.22559(15)	0.22011(2)	0.2217(10)	0.22150(18)	0.2233(8)	0.219(15)
z(D)	0.12161(47)	0.12041(3)	0.1196(10)	0.1199(4)	0.1209(15)	0.124(20)
x(O)	0.14839(3)	0.14888(1)	0.14891(11)	0.14901(11)	0.1488(5)	0.161(4)
y(O)	0.08264(3)	0.08073(1)	0.08070(11)	0.08096(10)	0.0810(5)	0.088(5)
z(O)	0.12584(5)	0.12643(2)	0.12566(11)	0.12577(13)	0.1260(5)	0.121(8)
UISO (O)	-	-	0.0183(12)	0.02612(4)	0.01755(5)	0.006(10)
UISO (D)	-	-	0.0279(8)	0.01664(5)	0.01709(8)	0.023(33)